Inorganic Chemistry
Article

Inorg. Chem. **2010**, *49*, 9777–9787 **9777**
DOI: 10.1021/ic1006296

Structural Distortions upon Oxidation in Heteroleptic [Cp_2W(dmit)] Tungsten Dithiolene Complex: Combined Structural, Spectroscopic, and Magnetic Studies

Eric W. Reinheimer,[†] Iwona Olejniczak,[‡] Andrzej Łapiński,[‡] Roman Świetlik,*[,‡] Olivier Jeannin,[†] and Marc Fourmigué*[,†]

[†]*Sciences Chimiques de Rennes, Université de Rennes I & CNRS UMR 6226, Campus de Beaulieu, 35042 Rennes, France, and* [‡]*Institute of Molecular Physics, Polish Academy of Sciences, ul. M. Smoluchowskiego 17, 60-179 Poznań, Poland*

Received April 6, 2010

Four different cation radical salts are obtained upon electrocrystallization of [Cp_2W(dmit)] (dmit = 1,3-dithiole-2-thione-4,5-dithiolato) in the presence of the BF_4^-, PF_6^-, Br^-, and $[Au(CN)_2]^-$ anions. In these formally d^1 cations, the WS_2C_2 metallacycle is folded along the S···S hinge to different extents in the four salts, an illustration of the noninnocent character of the dithiolate ligand. Structural characteristics and the charge distribution on atoms, for neutral and ionized complexes with various folding angles, were calculated using DFT methods, together with the normal vibrational modes and theoretical Raman spectra. Raman spectra of neutral complex [Cp_2W(dmit)] and its salts formed with BF_4^-, AsF_6^-, PF_6^-, Br^-, and $[Au(CN)_2]^-$ anions were measured using the red excitation (λ = 632.8 nm). A correlation between the folding angle of the metallacycle and the Raman spectroscopic properties is analyzed. The bands attributed to the C═C and C−S stretching modes shift toward higher and lower frequencies by about 0.3−0.4 cm^{-1} deg^{-1}, respectively. The solid state structural and magnetic properties of the three salts are analyzed and compared with those of the corresponding molybdenum complexes. Temperature dependence of the magnetic susceptibility shows the presence of one-dimensional antiferromagnetic interactions in the BF_4^-, PF_6^-, and $[Au(CN)_2]^-$ salts, while an antiferromagnetic ground state is identified in the Br^- salt below $T_{Néel}$ = 7 K. Interactions are systematically weaker in the tungsten salts than in the isostructural molybdenum analogs, a consequence of the decreased spin density on the dithiolene ligand in the tungsten complexes.

Introduction

Heteroleptic complexes associating cyclopentadienyl and dithiolene ligands, such as Cp_2Mo(dithiolene) complexes, are currently investigated, among other dithiolene complexes, as model compounds for molybdeno-enzymes.[1] Indeed, the enzyme function is directly correlated with the different redox states these complexes can adopt, from Mo^{IV} to Mo^{VI}, through the intermediate radical, formally the d^1 Mo^V species. The model Cp_2Mo(dithiolene) complexes represent in that respect a useful tool, as several formally d^1 Mo^V radical cations species were isolated and structurally investigated.[2−4] Of particular interest in these d^1 $[Cp_2Mo(dithiolene)]^{+\bullet}$ complexes is the variable folding of the MoS_2C_2 metallacycle along the S···S hinge (θ), which is associated with a stabilization of the oxidized form through a mixing of the Cp_2Mo d-type fragment orbital and the dithiolene π orbital. Accordingly, the d^0 complexes described with titanium for example are strongly folded ($\theta > 40°$) while the d^2 Mo or W complexes are not ($0 \leq \theta \leq 10°$).[5] Interestingly, a variety of folding angles ($0 \leq \theta \leq 30°$) was found for a given d^1 complex depending on the nature of the counterion and associated solid-state structure.[6] This folding, rationalized 20 years ago by Lauher and Hoffmann[7] on the basis of extended Hückel calculations, has been also investigated experimentally in detail by photoelectron spectroscopy (PES)[8,9] or EPR techniques.[10,11]

*To whom correspondence should be addressed. E-mail: swietlik@ifmpan.poznan.pl (R.Ś.), marc.fourmigue@univ-rennes1.fr (M.F.).

(1) McMaster, J.; Turner, J. M.; Garner, C. D. *Prog. Inorg. Chem.* **2004**, *52*, 539.
(2) (a) Fourmigué, M.; Domercq, B.; Jourdain, I. V.; Molinié, P.; Guyon, F.; Amaudrut, J. *Chem.—Eur. J.* **1998**, *4*, 1714. (b) Fourmigué, M.; Lenoir, C.; Coulon, C.; Guyon, F.; Amaudrut, J. *Inorg. Chem.* **1995**, *34*, 4979.
(3) (a) Clérac, R.; Fourmigué, M.; Gaultier, J.; Barrans, Y.; Albouy, P. A.; Coulon, C. *Eur. Phys. J. B* **1999**, *9*, 431. (b) Clérac, R.; Fourmigué, M.; Coulon, C. *J. Solid State Chem.* **2001**, *159*, 413.
(4) Domercq, B.; Coulon, C.; Fourmigué, M. *Inorg. Chem.* **2001**, *40*, 371.
(5) Fourmigué, M. *Coord. Chem. Rev.* **1998**, *178−180*, 823.
(6) Fourmigué, M. *Acc. Chem. Res.* **2004**, *37*, 179.
(7) Lauher, J. W.; Hoffmann, R. *J. Am. Chem. Soc.* **1976**, *98*, 1729.
(8) (a) Joshi, H. K.; Cooney, J. J. A.; Inscore, F. E.; Gruhn, N. E.; Lichtenberger, D. L.; Enemark, J. H. *Proc. Natl. Acad. Sci. U. S. A.* **2003**, *100*, 3719. (b) Cooney, J. J. A.; Cranswick, M. A.; Gruhn, N. E.; Joshi, H. K.; Enemark, J. H. *Inorg. Chem.* **2004**, *43*, 8110.
(9) Cranswick, M. A.; Dawson, A.; Cooney, J. J. A.; Gruhn, N. E.; Lichtenberger, D. L.; Enemark, J. H. *Inorg. Chem.* **2007**, *46*, 10639.
(10) Enemark, J. H.; Cooney, J. J. A.; Wang, J.-J.; Holm, R. H. *Chem. Rev.* **2004**, *104*, 1175.
(11) (a) Drew, S. C.; Young, C. G.; Hanson, G. R. *Inorg. Chem.* **2007**, *46*, 2388. (b) Drew, S. C.; Hill, J. P.; Lane, I.; Hanson, G. R.; Gable, R. W.; Young, C. G. *Inorg. Chem.* **2007**, *46*, 2373. (c) Drew, S. C.; Hanson, G. R. *Inorg. Chem.* **2009**, *48*, 2224.

Published on Web 09/30/2010

Scheme 1. Origin of the Folding of the MS_2C_2 Metallacycle in Cp_2M-(dithiolene) Complexes, Illustrated Here on W d^1 Complexes[a]

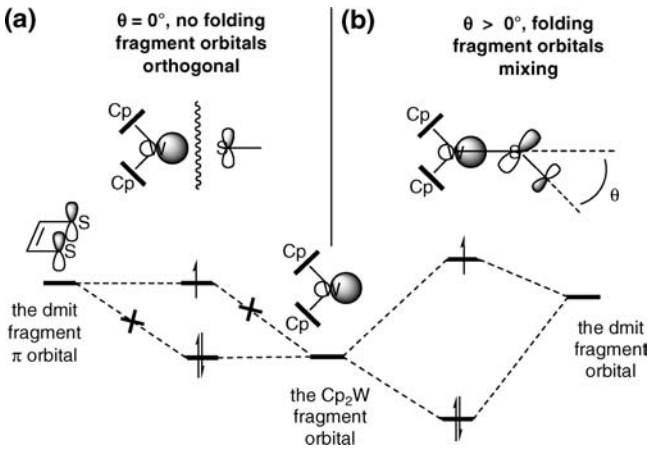

[a] No folding is found in d^2 complexes (4 e^-/2 orbitals). Systematic strong folding is found in d^0 species ($2e^-$/2 orbitals), variable folding in the intermediate formally d^1 complexes.

As shown in Scheme 1b, the SOMO of such radical complexes is then the antibonding combination of the Cp_2W d fragment orbital and the π-type dithiolene frontier orbital. Within this simple model, the interaction is strongest when the two fragment orbitals are closest in energy, giving rise to a SOMO essentially equally distributed on both fragments, hence the description of a *formal* d^1 electron count since part of the SOMO is also delocalized on the dithiolene ligand. The relative ordering of the two frontier orbitals plays an important role. Indeed, if now an electron-rich dithiolene ligand such as dmit is used, its π-type frontier orbital is higher in energy, and the SOMO has therefore stronger ligand character (and less metal character).[4]

In those rare situations where the radical complex is not folded at all (Scheme 1a, $\theta = 0°$), the two fragment orbitals are orthogonal and do not mix; the SOMO is then the highest of the two fragment orbitals. With an electron-rich dithiolate such as dmit, the unfolded radical could then be essentially localized on the dithiolene moiety.[3] In this case, the unfolded complexes can essentially be described as a d^2 Cp_2W moiety interacting with a radical dithiolene ligand, and the formal d^1 electron count description becomes a misuse of language.

IR-Raman spectroscopy provides another useful tool to investigate this folding in the oxidized species, as it is anticipated that an unfolded complex would concentrate most of the charge density on the dithiolene moiety, with associated important C−S shortening and C=C bond lengthening effects. On the other hand, a more folded complex with a larger spin density on the metal should exhibit weaker effects on the C−S and C=C, with their associated vibrational spectroscopy signatures. Actually, a clear-cut correlation in Mo complexes has been recently reported,[12] between the folding angle of the MoS_2C_2 metallacycle and the wavenumber of characteristic Raman bands such as the C=C and C−S stretching vibrations where this effect is strongest. The folding of $[Cp_2Mo(dmit)]^{+\bullet}$ cations was found to be related to a low-wavenumber shift ($0.5 - 0.6$ cm^{-1}/deg) of Raman bands assigned to the C=C and some C−S stretching vibrations. From a materials science point of view, these radical complexes are also of interest as the spin density distribution is directly dependent on the folding angle. With dithiolene ligands such as those used for the elaboration of square-planar conducting salts,[13] that is, $dmit^{2-}$ (dmit: 1,3-dithiole-2-thione-4,5-dithiolato) or $dddt^{2-}$ (5,6-dihydro-1,4-dithiine-2,3-dithiolato), the molybdenum complexes, in their radical form, $[Cp_2Mo(dmit)]^{+\bullet}$ or $[Cp_2Mo(dddt)]^{+\bullet}$, were shown to adopt different folding angles in the solid state between 0 and 30°, depending on the nature of the counterion, revealing a high flexibility with an associated variable spin density delocalization.[14]

By analogy with the extensive work performed on molybdenum dithiolene complexes as models of Mo enzymes,[1] several mono-[15,16] or bis(dithiolene) tungsten complexes[17−19] have been also described to date as models[20,21] for corresponding tungsten enzymes.[22,23] The latter are particularly interesting as they are essentially observed in thermophilic or hyperthermophilic microorganisms, by contrast with the molybdenum enzymes found in mesophilic ones. Several explanations have been proposed for the actual preference for one or another metal at the active sites of the enzymes,[24,25] such as for example stronger $\pi-\pi$ interactions between sulfur and metal atoms in the tungsten complexes.[25b] Differences of redox potentials of the Mo and W $O{=}M(dithiolene)_2^{2-/1-}$ complexes were also addressed.[26] Recently, Schulzke demonstrated that the electrochemical properties of several pairs of Mo and W complexes showed huge differences in the response of their redox potential to temperature changes.[27] The higher

(12) Świetlik, R.; Łapiński, A.; Fourmigué, M.; Yakushi, K. *J. Raman Spectrosc.* **2009**, *40*, 2092–2098.

(13) Kato, R. *Chem. Rev.* **2004**, *104*, 5319.
(14) Fourmigué, M. *Top. Organomet. Chem.* **2009**, *27*, 161.
(15) (a) Wang, J.-J.; Groysman, S.; Lee, S. C.; Holm, R. H. *J. Am. Chem. Soc.* **2007**, *129*, 7512. (b) Groysman, S.; Wang, J.-J.; Tagore, R.; Lee, S. C.; Holm, R. H. *J. Am. Chem. Soc.* **2008**, *130*, 12794. (c) Groysman, S.; Majumdar, A.; Zheng, S.-L.; Holm, R. H. *Inorg. Chem.* **2010**, *49*, 1082.
(16) (a) Sproules, S. A.; Morgan, H. T.; Doonan, C. J.; White, J. M.; Young, C. G. *Dalton Trans.* **2005**, 3552. (b) Eagle, A. A.; George, G. N.; Tiekink, E. R. T.; Young, C. G. *J. Inorg. Biochem.* **1999**, *76*, 39. (c) Eagle, A. A.; Harben, S. M.; Tiekink, E. R. T.; Young, C. G. *J. Am. Chem. Soc.* **1994**, *116*, 9749.
(17) (a) Ueyama, N.; Oku, H.; Nakamura, A. *J. Am. Chem. Soc.* **1992**, *114*, 7310. (b) Stewart, L. J.; Bailey, S.; Bennett, B.; Charnock, J. M.; Garner, C. D.; McAlpine, A. S. *J. Mol. Biol.* **2000**, *299*, 593.
(18) (a) Donahue, J. P.; Lorber, C.; Nordlander, E.; Holm, R. H. *J. Am. Chem. Soc.* **1998**, *120*, 3259. (b) Donahue, J. P.; Goldsmith, C. R.; Nadiminti, U.; Holm, R. H. *J. Am. Chem. Soc.* **1998**, *120*, 12869. (c) Lorber, C.; Donahue, J. P.; Goddard, C. A.; Nordlander, E.; Holm, R. H. *J. Am. Chem. Soc.* **1998**, *120*, 8102.
(19) (a) Sung, K.-M.; Holm, R. H. *J. Am. Chem. Soc.* **2001**, *123*, 1920. (b) Sung, K.-M.; Holm, R. H. *Inorg. Chem.* **2001**, *40*, 4518. (c) Goddard, C. A.; Holm, R. H. *Inorg. Chem.* **1999**, *38*, 5389. (d) Lim, B. S.; Holm, R. H. *J. Am. Chem. Soc.* **2001**, *123*, 1920.
(20) (a) Das, S. K.; Biswas, D.; Maiti, R.; Sarkar, S. *J. Am. Chem. Soc.* **1996**, *118*, 1387. (b) Yadav, J.; Das, S. K.; Sarkar, S. *J. Am. Chem. Soc.* **1997**, *119*, 4315.
(21) (a) Sugimoto, H.; Tajima, R.; Sakurai, T.; Ohi, H.; Miyake, H.; Itoh, S.; Tsukube, H. *Angew. Chem., Int. Ed.* **2006**, *45*, 3520. (b) Sugimoto, H.; Tano, H.; Toyota, K.; Tajima, R.; Miyake, H.; Takahashi, I.; Hirota, S.; Itoh, S. *J. Am. Chem. Soc.* **2010**, *132*, 8.
(22) Stewart, L. J.; Bailey, S.; Bennet, B.; Charnock, J. M.; Garner, C. D.; McAlpine, A. S. *J. Mol. Biol.* **2000**, *299*, 593.
(23) (a) Oku, H.; Ueyama, N.; Kondo, M.; Nakamura, A. *Inorg. Chem.* **1994**, *33*, 209. (b) Helton, M. E.; Gebhart, N. L.; Davis, E. S.; McMaster, J.; Garner, C. D.; Kirk, M. L. *J. Am. Chem. Soc.* **2001**, *123*, 10389.
(24) de Bok, F. A. M.; Hagedoorn, P.-L.; Silva, P. J.; Hagen, W. R.; Schiltz, E.; Fritsche, K.; Stams, A. J. M. *Eur. J. Biochem.* **2003**, *270*, 2476.
(25) (a) Hochheimer, A.; Linder, D.; Thauer, R. K.; Hedderich, R. *Eur. J. Biochem.* **1995**, *234*, 910. (b) Johnson, M. K.; Rees, D. C.; Adams, M. W. W. *Chem. Rev.* **1996**, *96*, 2817.
(26) Tucci, G. C.; Donahue, J. P.; Holm, R. H. *Inorg. Chem.* **1998**, *37*, 1602.
(27) Schulzke, C. *Dalton Trans.* **2005**, 713. (b) Döring, A.; Schulzke, C. *Dalton Trans.* **2010**, *39*, 5623.

temperature sensitivity of the redox properties of the W complexes was associated with more severe geometric changes upon oxidation which might increase the protein's reorganization energies needed. If we consider the simple monodithiolene complexes formulated as Cp_2W(dithiolene), a few neutral examples were described with benzenedithiolate (bdt) or toluenedithiolate (tdt) ligands,[28] and more recently with the sulfur-rich dddt and dmit ligands.[29] However, among them, only a very limited number of formally d^1, oxidized species were described, limiting the identification of systematic trends, for comparison with the analogous Mo complexes. Indeed, the only two structurally characterized examples of d^1 W complexes, that is, $[Cp_2W(dmit)]^+$ in its AsF_6^- and $TCNQF_4^-$ salts, exhibit very different geometries with folding angles of 0 and 27.56(1)°, respectively.[4,2a]

In order to establish whether such tungsten complexes are indeed more prone to larger geometrical modifications upon oxidation, as suggested by earlier electrochemical[27] and theoretical studies,[4] we decided to expand the family of such open-shell d^1 tungsten derivatives and prepared four novel salts of the $[Cp_2W(dmit)]^{+\bullet}$ radical cation with, respectively, the BF_4^-, the PF_6^-, the Br^-, and the $[Au(CN)_2]^-$ anions. The geometry adopted by the complexes in the four crystalline salts, and particularly the different folding angles of the WS_2C_2 metallacycle, have been correlated to their vibrational spectra, through the specific evolution of the C−S and C=C Raman signatures. Furthermore, the solid state structures adopted by the four salts have been analyzed in detail to rationalize the observed magnetic behaviors investigated by the temperature dependence of the magnetic susceptibility. This extended set of radical tungsten complexes allows now for interesting comparisons, within the series as well as with the analogous molybdenum complexes, as described below.

Results and Discussion

Molecular structures. $[Cp_2W(dmit)]$ was prepared from the reaction of Cp_2WCl_2 and $(Na^+)_2(dmit^{2-})$ as reported elsewhere.[2,4] Its galvanostatic electrocrystallization in the presence of $[n\text{-}Bu_4N][BF_4]$, $[n\text{-}Bu_4N][PF_6]$, $[PPh_4][Br]$, or $[n\text{-}Bu_4N][Au(CN)_2]$ afforded black crystals on the anode. It should be stressed indeed that this electrocrystallization technique[30] is not limited to the crystal growth of conducting materials but is also well suited for the crystallization of insulating magnetic salts such as those described here, when the proper conditions for crystallization are met. Single crystal X-ray diffraction experiments were performed on the four salts. The BF_4^- and the PF_6^- salts are isostructural (monoclinic, space group $P2_1/c$), with both the cation and anion in general position in the unit cell. The only difference between the two salts is a disorder which affects one Cp ring and the BF_4^- anion in $[Cp_2W(dmit)][BF_4]$, while no disorder is found in the PF_6^- salt. The two other salts with Br^- and $[Au(CN)_2]^-$ crystallize respectively in the monoclinic system, space group $P2_1/c$, and the orthorhombic system, space group $P2_12_12_1$. In the following, we will first describe the molecular geometry evolutions within these series together with their Raman spectroscopic properties, and we will discuss in a second part the solid state structures these radical species adopt in the solid state and the correlation with their magnetic behavior.

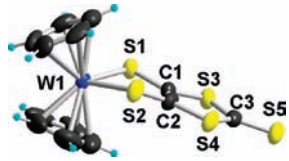

Figure 1. View of the cation radical $[Cp_2W(dmit)]^{+\bullet}$ in its PF_6^- salt. Note the folding of the WS_2C_2 metallacycle along the S1···S2 hinge. Ellipsoids are shown at the 50% probability level.

As shown in Figure 1, the cation radical $[Cp_2W(dmit)]^{+\bullet}$ species adopts a recurrent geometry with a characteristic distortion of the WS_2C_2 metallacycle through a folding along the S1···S2 hinge. The most pertinent geometrical features (bond distances and angles, folding angle) of the cation in the four salts are collected in Table 1, together with those of two salts reported earlier with $TCNQF_4$ and with AsF_6^-. The $[Cp_2W(dmit)]^{+\bullet}$ cation in the four salts exhibits a comparable folding angle of the metallacycle, 27.71(9)° in the BF_4^- salt, 26.8(2)° in the PF_6^- salt, 31.55(7)° in the Br^- salt, and 29.7(2) and 31.7(2)° in the two crystallographically independent molecules in the $[Au(CN)_2]^-$ salt. Comparison of the C=C and C−S bond lengths with those found earlier in the unfolded AsF_6^- salt are particularly interesting (Table 1). Indeed, the folded complexes systematically exhibit a shorter C=C bond and longer C−S bonds, indicating that the oxidation affects the dithiolene ligand to a smaller extent in the folded complexes.

An interesting comparison can be also made with the analogous molybdenum salts (Table 2). Indeed, the corresponding $[Cp_2Mo(dmit)]^{+\bullet}$ salts have been reported with all except the $[Au(CN)_2]^-$ anion. It appears that the salts with Mo and W are not systematically isostructural and that, even when they are, the folding angles are systematically larger in the tungsten than in the molybdenum complexes. This trend has been attributed to a stronger interaction between the Cp_2M and dmit frontier orbitals when M = W.[2a,4]

DFT Calculations. Quantum chemical calculations for tungsten complexes were performed at the B3LYP/LanL2DZ theory level, as previously described for the molybdenum complexes.[12] The geometry optimization of the neutral complex and its radical cation $[Cp_2W(dmit)]^{+\bullet}$ gave an almost undistorted geometry (in both cases $\theta = 2.8°$). Upon complex ionization, the length of the metallacycle C=C bond increases while the C−S inner bonds connected with the C=C bond decrease their lengths (Table 3). Subsequently, we optimized the geometry of the $[Cp_2W(dmit)]^{+\bullet}$ cation by fixing different folding angles (θ = 10°, 20°, 30°). The bond analysis shows that on folding, all the C−S bonds grow, while the C=C and C=S bonds decrease in length. Such modifications are in agreement with the above-reported X-ray crystallographic data. Additionally, the average charge on the different atoms of the neutral complex and its cation with different folding

(28) (a) Green, M. L. H.; Lindsell, W. E. *J. Chem. Soc.* **1967**, 1455. (b) Debaerdemaeker, T.; Kutoglu, A. *Acta Crystallogr., Sect. B* **1973**, *29*, 2664. (c) Lindsell, W. E. *J. Chem. Soc., Dalton Trans.* **1975**, 2548. (d) Klapoetke, T.; Koepf, H. *Z. Anorg. Allg. Chem.* **1988**, *558*, 217.

(29) (a) Jourdain, I. V.; Fourmigué, M.; Guyon, F.; Amaudrut, J. *J. Chem. Soc., Dalton Trans.* **1998**, 483. (b) Jourdain, I. V.; Fourmigué, M.; Guyon, F.; Amaudrut, J. *Organometallics* **1999**, *18*, 1834.

(30) Batail, P.; Boubekeur, K.; Fourmigué, M.; Gabriel, J.-C. P. *Chem. Mater.* **1998**, *10*, 3005.

Table 1. Important Bond Distances and Angles in the Different $[Cp_2W(dmit)]X$ Salts[a]

counter ion		M−S (Å)	C−S (Å)	C=C (Å)	S−M−S (deg)	θ (deg)	ref
BF_4^-		2.4136(15)	1.718(3)	1.380(8)	83.13(5)	27.71(9)	this work
		2.4317(16)	1.723(3)				
PF_6^-		2.408(4)	1.709(9)	1.374(11)	82.94(7)	26.8(2)	this work
		2.422(6)	1.714(8)				
Br^-		2.4330(9)	1.725(3)	1.379(4)	82.98(3)	31.55(7)	this work
		2.4343(9)	1.718(3)				
$[Au(CN)_2]^-$	mol 1	2.427(2)	1.719(8)	1.366(12)	82.89(9)	31.7(2)	this work
		2.423(3)	1.717(9)				
	mol 2	2.426(3)	1.718(9)	1.348(12)	83.56(8)	29.7(2)	
		2.425(2)	1.731(9)				
$TCNQF_4^-$		2.426(4)	1.721(6)	1.374(8)	83.18(5)	27.56(1)	2a
		2.441(4)	1.722(6)				
AsF_6^-		2.429(1)	1.693(5)	1.384(9)	83.86(7)	0	4

[a] The torsion angle θ represents the angle between the WS_2 and S_2C_2 mean planes of the WS_2C_2 metallacycle.

Table 2. Folding Angles of the Metallacycle in Various Salts of $[Cp_2Mo(dmit)]$ and $[Cp_2W(dmit)]$

counter ion	θ_{Mo}	ref_{Mo}	θ_W	ref_W	Mo vs. W
BF_4^-	23.21(5)	3b	27.71(9)	this work	isostructural
PF_6^-	0	3a	26.8(2)	this work	different
Br^-	30.45(4)	3b	31.55(7)	this work	isostructural
$TCNQF_4^-$	10.2(1)	2a	27.56(1)	2a	different
AsF_6^-	0	3a	0	4	isostructural

Table 3. Calculated Bond Lengths of Neutral and Ionized $Cp_2W(dmit)$ Complex for Various Folding Angles (θ), at the B3LYP/LanL2DZ Theory Level (Atom Labeling Is Given in Figure 1)

		radical cation			
compound folding angle	neutral	0°	10°	20°	30°
C1−S1	1.823	1.778	1.779	1.784	1.789
C2−S2	1.820	1.778	1.779	1.784	1.789
C1=C2	1.350	1.397	1.396	1.392	1.388
C1−S3	1.827	1.807	1.808	1.809	1.809
C2−S4	1.828	1.807	1.808	1.809	1.809
C3−S3	1.824	1.837	1.837	1.839	1.841
C3−S4	1.824	1.837	1.837	1.839	1.841
C3=S5	1.684	1.662	1.662	1.662	1.662

Table 4. Charge Distribution (Mulliken) on Atoms of Neutral and Ionized $Cp_2W(dmit)$ Complex with Various Folding Angles (θ) Calculated at the B3LYP/LanL2DZ Theory Level (Atom Numbering Is Given in Figure 1)

		$[Cp_2W(dmit)]^{+\bullet}$ cation			
atom	neutral complex	θ = 0°	θ = 10°	θ = 20°	θ = 30°
S1	0.162	0.297	0.299	0.270	0.280
S2	0.127	0.259	0.263	0.306	0.314
C1	−0.322	−0.317	−0.309	−0.316	−0.331
C2	−0.313	−0.307	−0.318	−0.325	−0.338
S3	0.385	0.481	0.446	0.440	0.435
S4	0.352	0.449	0.478	0.473	0.468
C3	−0.611	−0.609	−0.609	−0.611	−0.612
S5	0.013	0.189	0.185	0.178	0.171
$\sum(C_3S_5)$	−0.207	0.442	0.435	0.415	0.387
W	−0.594	−0.664	−0.670	−0.685	−0.689
$\sum(Cp_2W)$	0.207	0.558	0.565	0.585	0.613

angles was evaluated (Table 4). Going from the neutral complex to the radical cation species, we first observe that a large part of positive charge is transferred to the dithiolene moiety, illustrating the important contribution of the dithiolene moiety in the oxidation. Furthermore, upon $[Cp_2W(dmit)]^{+\bullet}$ cation folding, this average positive charge on dmit actually decreases by about 11%, when bending the cation from 0° to 30°, showing that this

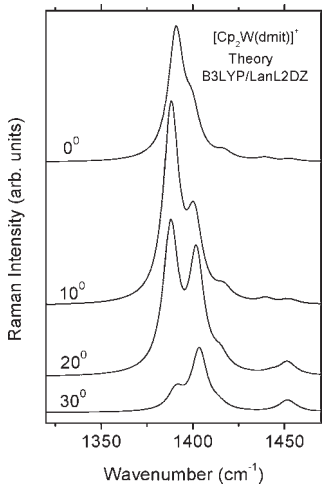

Figure 2. Theoretical Raman spectra within the C=C stretching for the $[Cp_2W(dmit)]^{+\bullet}$ cation, calculated for different folding angles at the B3LYP/LanL2DZ theory level (non-normalized data).

dithiolene contribution decreases upon folding. While analogous modifications of the bond lengths upon complex folding were also observed in the case of the $[Cp_2Mo(dmit)]^{+\bullet}$ cation, the charge decrease on the dmit ligand for the $[Cp_2Mo(dmit)]^{+\bullet}$ cation upon bending from 0° to 30° was found to be much smaller (about 0.5%).

We have also calculated the frequencies of vibrational modes and Raman scattering intensities for both neutral and ionized complexes with different folding angles. The mode description was done by visual inspection of each individual mode by using the GaussView program. For the neutral $[Cp_2W(dmit)]$ complex, one C=C stretching mode is seen, and it exhibits a strong low-frequency shift upon ionization (about 70 cm^{-1}). For the $[Cp_2W(dmit)]^{+\bullet}$ cation, we have found two vibrational modes related to the C=C stretching (Figure 2). The visual inspection of these modes shows that in the case of the radical cation, in addition to the C=C stretching, the Cp groups also perform vibrations which are different for each C=C mode. This contribution of the Cp groups to the C=C vibration modes of the $[Cp_2W(dmit)]^{+\bullet}$ cation is not observed in the neutral complex. On cation folding from θ = 0° to θ = 30°, the lower-frequency C=C mode shows nearly no shift, while the higher-frequency one shifts up by about 4 cm^{-1}. Simultaneously, the related Raman bands change their theoretical intensities. It should be emphasized here

that for the $[Cp_2Mo(dmit)]^{+\bullet}$ cation investigated earlier, only one C=C mode was found, and the related Raman band showed a low-frequency shift upon folding.[12] The folding of the $[Cp_2W(dmit)]^{+\bullet}$ cation by about $\theta = 30°$ also has an influence on other vibrational stretching modes: the C=S mode shifts up by 4 cm^{-1} and the C−S modes shift up or down depending on the mode, while the frequency W−S mode is nearly constant.

Experimental Raman Spectra. Raman spectra of the $[Cp_2W(dmit)]X$ salts were measured on single crystals for the electrical vector parallel and perpendicular to the direction of the maximum C=C band intensity. The spectra of the various salts were similar. As an example, we show the spectra of the $[Cp_2W(dmit)]BF_4$ salt within the region of strongest vibrational features (Figure 3). The spectra of all the salts and also the neutral complex, for polarization corresponding to the maximum C=C band intensity, are displayed in Figure 4, and positions of the most important bands are listed in Table 6. While the DFT calculations of the $[Cp_2W(dmit)]^{+\bullet}$ cation revealed the existence of two vibrational modes attributed to the C=C bond stretching, our analysis of the experimental data shows only one Raman line for all studied salts. Apparently, in crystals, these modes have almost the same frequencies, and they cannot be distinguished in our Raman experiments, at room temperature at least. On cation folding from $\theta = 0°$ (in AsF_6^- salt) to 27−32° (in the four other salts), the C=C band exhibits a shift of approximately 10 cm^{-1} toward higher frequencies (Table 5). This observation is in agreement with the tendency suggested by the theoretical calculations, which show that the high-frequency C=C mode increases its frequency and relative intensity. Consequently, the band, being a superposition of these two components, should shift toward higher frequencies. It is important to note that the behavior of the C=C mode in the $[Cp_2W(dmit)]^{+\bullet}$ cation is different from that of the $[Cp_2Mo(dmit)]^{+\bullet}$ cation, where the folding actually decreased the frequency of the C=C mode.[12]

The most important changes induced by folding are observed for Raman bands related to C−S stretching at about 920 cm^{-1}: they exhibit a low-frequency shift of about 10 cm^{-1}, from the unfolded AsF_6^- salt to the strongly folded salts ($\theta = 27-32°$). A slightly larger (about 15 cm^{-1}) frequency shift had been observed for the $[Cp_2Mo(dmit)]^{+\bullet}$ cation.[12] It therefore clearly appears that the C−S band at about 920 cm^{-1} is probably the best indicator of metallacycle distortion in both Mo and W complexes in the solid state.

In conclusion, by comparison with the unfolded AsF_6^- salt, the theoretical calculations and Raman data show that the strong folding observed in the W complexes described here is associated with a transfer of the oxidation site, from the dithiolene ligand to the Cp_2W moiety. From a magnetic point of view, this should be associated with a decreased spin density on the dithiolene ligand. To address this point, we will therefore describe in the following the solid-state magnetic response of these four salts. Indeed, while a wide variety of structures and magnetic behaviors has been reported for analogous molybdenum complexes,[6,14] very few examples involving tungsten complexes have been reported to date, with $[Cp_2W(dmit)]$ as mentioned above,[2a,4] with $[Cp_2W(dmid)]$ (dmid: 1,3-dithiole-2-one-4,5-dithiolato),[2a] and with the

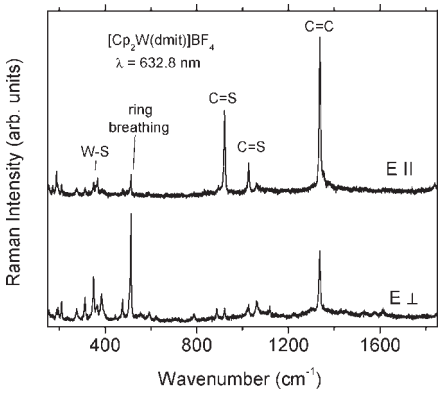

Figure 3. Raman spectra of the $[Cp_2W(dmit)]BF_4$ salt recorded for two different orientations of the electrical vector of the exciting laser beam ($\lambda = 632.8$ nm): parallel ($E_{||}$) and perpendicular ($E_\perp$) to the maximum intensity of the band assigned to the C=C stretching vibration.

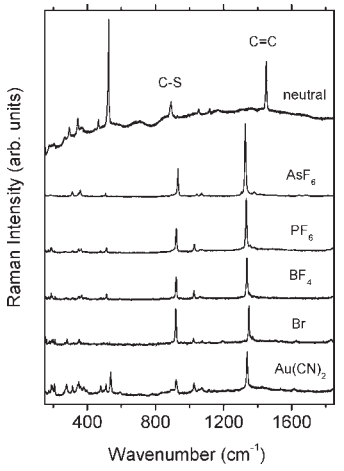

Figure 4. Raman spectra of the neutral $Cp_2W(dmit)$ complex and $[Cp_2W(dmit)]X$ salts (X = AsF_6, PF_6, BF_4, Br, $Au(CN)_2$) obtained at room temperature using red excitation ($\lambda = 632.8$ nm). The electrical vector of the laser beam was parallel to the direction of the maximum C=C band intensity.

Table 5. Selected Raman Bands of the Neutral $Cp_2W(dmit)$ and Its Radical Cation in $[Cp_2W(dmit)]X$ Salts, X = AsF_6, PF_6, BF_4, Br, and $Au(CN)_2$, Recorded with Excitation $\lambda = 632.8$ nm

compound	neutral	AsF_6^-	PF_6^-	BF_4^-	Br^-	$Au(CN)_2^-$	assignement
folding angle (θ)		0.0	26.8(2)	27.71(9)	31.55(7)	31.7(2), 29.7(2)	
Raman bands	1451	1329	1334	1337	1348	1339	C=C stretching
	1053	1042	1028	1022	1024	1026	C=S stretching
	891, 886	932	922	922	920	922	C−S stretching
	523	508	513	513	516	509	C−S stretching (ring breathing)
	464	482	476	477	475	479	C−S stretching
	344	358, 346	364, 349	365, 349	366, 351	361, 350	W−S stretching

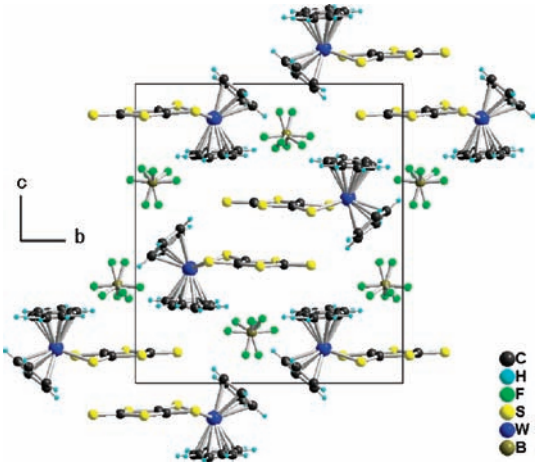

Figure 5. Projection view along *a* of the unit cell of $[Cp_2W(dmit)]BF_4$. The BF_4^- anion is disordered on two positions.

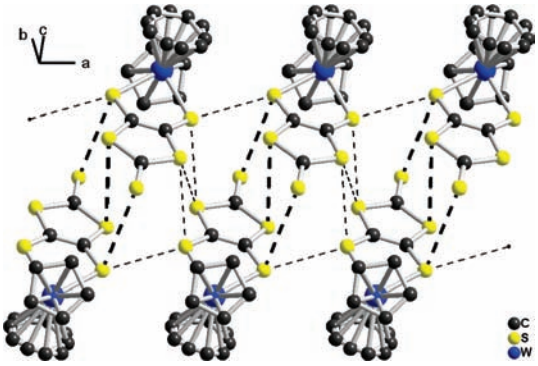

Figure 6. View of the chains of cation radical dyads running along *a* in $[Cp_2W(dmit)]BF_4$. The thick dotted lines indicate the strongest intermolecular interaction between molecules at (x, y, z) and $(1 - x, -y, 2 - z)$.

diselenolene complex $[Cp_2W(dsit)]$ (dsit: 1,3-dithiole-2-thione-4,5-diselenato).[2a,4] The four novel salts reported here give an opportunity to expand these series, allowing now for pertinent comparisons, between the different W salts as well as with the analogous molybdenum ones, as detailed below.

$[Cp_2W(dmit)]BF_4$. The $[Cp_2W(dmit)]BF_4$ salt crystallizes in the monoclinic system, space group $P2_1/c$, with both the cation and anion in general positions in the unit cell. A projection view along *a* (Figure 5) shows that the radical cations are organized into dyads with a face-to-face σ overlap of the dmit moieties and short S···S contacts (3.50−3.57 Å), while these dyads interact sideways along *a* with larger S···S contacts at 3.70 Å. In order to evaluate the extent of interactions within the dyad and between dyads along *a*, calculations of the $\beta_{HOMO-HOMO}$ interactions energies were performed in the frame of extended Hückel tight binding methods.[31,32] The intradimer interaction shown with thick dotted lines in Figure 6 between molecules (x, y, z) and $(1 - x, -y, 2 - z)$ amounts to 0.086 eV, while the other face-to-face interaction with molecule $(-x, -y, 2 - z)$ amounts to 0.030 eV and the interaction along *a* with molecule $(1 + x, y, z)$ or $(-1 + x, y, z)$ amounts to 0.024 eV. The system can therefore be described as antiferromagnetic coupled dyads further interacting with neighboring molecules along *a*.

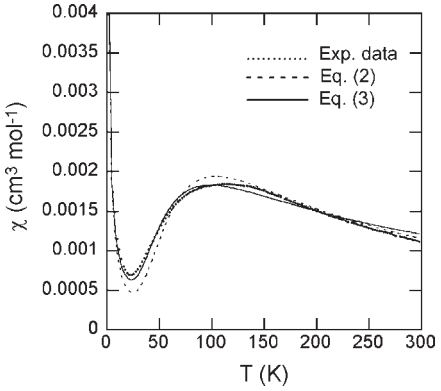

Figure 7. Temperature dependence of the magnetic susceptibility of $[Cp_2W(dmit)]BF_4$ at 5000 G. The dotted and solid lines are the best fits obtained by using eqs 2 ($R = 0.959$) and 3 ($R = 0.989$), respectively (see text).

The temperature dependence of the magnetic susceptibility (Figure 7) shows an activated regime at low temperatures with a susceptibility maximum around 100 K. Considering the structural description of this salt, the susceptibility data should be described with the theoretical expression for the magnetic susceptibility of an antiferromagnetically coupled $S = 1/2$ dimer with a singlet ground state, that is, the Bleaney−Bower equation, which reads per complex as

$$\chi_{BB} = \frac{Ng^2\beta^2}{k_B T(3 + \exp(-2J/k_B T))} \quad (1)$$

A second contribution observed at the lowest temperatures is attributed to magnetic defects whose contribution follows a Curie−Weiss behavior. Considering these two contributions, the susceptibility was accordingly fitted (dotted line in Figure 7) with the following expression:

$$\chi = \rho \frac{N\beta^2}{k_B(T - \theta)} + (1 - \rho)\chi_{BB} + \chi_{dia} \quad (2)$$

where χ_{dia} is the diamagnetic contribution and ρ, the fraction of paramagnetic impurities. We observe that the fit is not satisfactory (correlation coefficient $R = 0.959$), with the best set of parameters found to be $\chi_{dia} = 4.7(1) \times 10^{-5}$ cm^3 mol^{-1}, $\rho = 0.022$. and $J/k_B = -85(2)$ K. In order to perform a better description of the systems, the weaker interactions between dyads were taken into consideration in the model by the mean-field approximation,[33] with

$$\chi = \rho \frac{N\beta^2}{k_B(T - \theta)} + (1 - \rho)\frac{\chi_{BB}}{1 - (4zJ'\chi_{BB}/Ng^2\beta^2)} + \chi_{dia} \quad (3)$$

(31) Whangbo, M.-H.; Hoffmann, R. *J. Am. Chem. Soc.* **1978**, *100*, 6093. (b) Hoffmann, R. *J. Chem. Phys.* **1963**, *39*, 13978.

(32) Ren, J.; Liang, W.; Whangbo, M.-H. *Crystal and Electronic Structure Analysis Using CAESAR*; PrimeColor Software: http://www.primec.com/ (accessed Sep 2010), 1998.

(33) (a) Myers, B. E.; Berger, L.; Friedberg, S. *J. Appl. Phys.* **1969**, *40*, 1149. (b) Marsh, W. E.; Patel, K. C.; Hatfield, W. E.; Hodgson, D. J. *Inorg. Chem.* **1982**, *22*, 511.

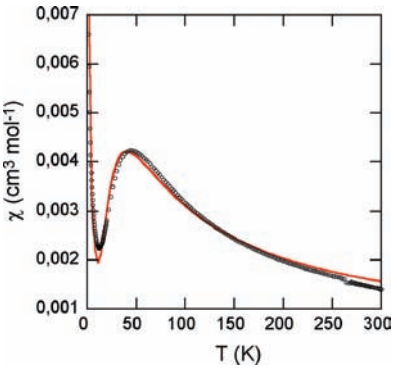

Figure 8. Temperature dependence of the magnetic susceptibility of $[Cp_2W(dmit)]PF_6$ at 5000 G. The solid line is the best fit obtained by using eq 3 (R = 0.982).

where z is the number of nearest next neighbors (z = 3) and J' is the average of interdimer magnetic exchange constants. A much improved agreement with the experimental data was obtained with this fit (full line in Figure 7), with the following set of parameters: $\chi_{dia} = 2.2(1) \times 10^{-5}$ cm^3 mol^{-1}, ρ = 0.02, $J_W/k_B = -82(1)$ K, and $J_W'/k_B = -7.8(4)$ K. It should be stressed here that very similar behavior was observed in the isostructural molybdenum salt, $[Cp_2Mo(dmit)](BF_4)$,[3b] albeit the interactions were notably stronger in the latter ($J_{Mo}/k_B = -145$ K, $J_{Mo}'/k_B = -15$ K). This trend has been already noticed in other salts known with both Mo and W metal centers.[34] It finds its origin in the stronger interaction between the Cp_2W and dmit fragment orbitals, which are closer in energy than in the Cp_2Mo/dmit situation. As a consequence, the folding angles are often larger in the tungsten complexes, and the HOMO of the cation radical species, which is the antibonding combination of both fragment orbitals, has a stronger metal character in the W complex and hence lesser dithiolene character. Since the dominant intermolecular interactions are actually based on the dmit/dmit interactions, these are decreased in the tungsten salts, when compared with isostructural molybdenum analogs.

$[Cp_2W(dmit)]PF_6$. As the BF_4^- and PF_6^- salts are isostructural, they exhibit an identical solid state organization (Figure 5), with radical cations associated into inversion-centered dyads with face-to-face interactions between the dmit moieties, with these dyads further interacting sideways along a. The temperature dependence of the magnetic susceptibility (Figure 8) exhibits a very similar behavior, without any field dependence, and with a susceptibility maximum observed at a lower temperature, which is 45 K vs 115 K in the BF_4^- salt. This clearly indicates that the antiferromagnetic interactions in the PF_6^- salt are strongly decreased, as also evidenced from the value of the J exchange constant determined from the same fit as above (eq 3). We found indeed the following set of parameters: χ_{dia} = 4.4 (1) 10^{-4} cm^3 mol^{-1}, ρ = 0.036, $J_W/k_B = -34.9(6)$ K, $J_W'/k_B = -3.6(2)$ K, with therefore an intradyad exchange constant J_W/k_B around -35 K, to be compared with -82 K in the BF_4^- salt. These decreased interactions reflect a negative pressure effect attributable to the larger size of the PF_6^- anion when compared with the BF_4^- one. Indeed, albeit isostructural, the two salts have different unit cell volumes, 1721.8(7) Å^3 in the BF_4^- salt and 1818.9(3) Å^3 in the PF_6^- salt. As a consequence, the radical cations are pushed apart from each other in the PF_6^- salt; the shortest intermolecular S···S contacts exceed 3.67 Å while they were found at 3.50 Å in the BF_4^- salt. Calculations of the $\beta_{HOMO-HOMO}$ interaction energies confirm this assumption, with the calculated intradyad interaction between (x, y, z) and ($1 - x$, $-y$, $2 - z$) (see Figure 6) found at 0.059 eV, to be compared to 0.086 eV in the BF_4^- salt.[35] If these values could at first sight appear relatively close to each other, one should recall that, in a Hubbard model,[36] with U describing the on-site electronic repulsion and β the resonance integral, the exchange integral J between two adjacent radicals is written as β^2/U. Thus, we expect the ratio $J(BF_4)/J(PF_6)$ to behave approximately as $[\beta(BF_4)/\beta(PF_6)]^2$. We find indeed $J(BF_4)/J(PF_6)$ = 2.3 and $[\beta(BF_4)/\beta(PF_6)]^2$ = 2.1.

Note also that a similar, isostructural but even more expanded structure was reported earlier in the diselenolene analog with the larger AsF_6^- anion, that is, $[Cp_2W(dsit)][AsF_6]$, where the cell volume amounted to 1932.6(3) Å^3.[4] In this salt, sizable antiferromagnetic interactions were reported with a susceptibility maximum at 78 K, indicating that the cell expansion effect was counterbalanced by the stronger overlap offered by the selenium atoms.

$[Cp_2W(dmit)]Br$. The structure of the bromide salt, $[Cp_2W(dmit)]Br$, is completely different; it crystallizes in

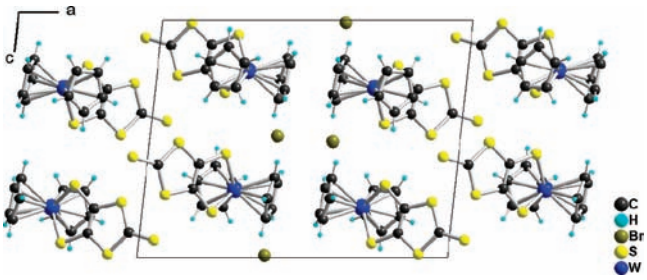

Figure 9. Projection view along b of the unit cell of $[Cp_2W(dmit)]Br$.

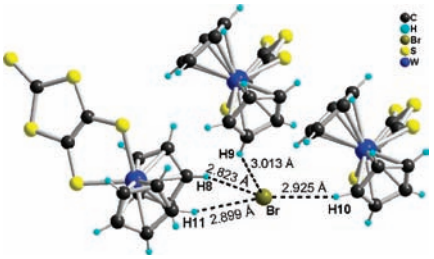

Figure 10. Detail of the hydrogen bond pattern around the Br^- anion in $[Cp_2W(dmit)]Br$.

Table 6. C−H···Br Hydrogen Bond Characteristics in $[Cp_2W(dmit)]Br$

interaction	(C−)H···Br/Å	C(−H)···Br/Å	C−H···Br/deg
Br···H8	2.823	3.72(5)	163.4(2)
Br···H11	2.899	3.803(5)	164.2(3)
Br···H10	2.925	3.817(7)	161.3(3)
Br···H9	3.013	3.780(5)	140.8(3)

(34) (a) Fourmigué, M.; Coulon, C. *Adv. Mater.* **1994**, *6*, 948. (b) Domercq, B.; Coulon, C.; Feneyrou, P.; Dentan, V.; Robin, P.; Fourmigué, M. *Adv. Funct. Mater.* **2002**, *12*, 359.

(35) The two others interactions (x, y, z)/($-x$, $2 - y$, $1 - z$) and (x, y, z)/($1 + x$, y, z) are found at 0.025 and 0.036 eV, respectively.

(36) Whangbo, M.-H. *Acc. Chem. Res.* **1983**, *16*, 95.

Table 7. Calculated $\beta_{HOMO-HOMO}$ Interactions Energies between One Complex at the (x, y, z) Position and Its Neighbors in [Cp_2W(dmit)]Br

complex at	interaction	β (meV)
(x, 1.5 − y, −0.5 + z) and (x, 1.5 − y, 0.5 + z)	S···S	37.4
(−x, 1 − y, 1 − z)	S···S	6.4
(−x, 2 − y, 1 − z)	S···S	9.7
(−x, −0.5 + y, 1.5 − z) and (−x, 0.5 + y, 1.5 − z)	S···S	21.6
(x, 1 + y, z) and (x, −1 + y, z)	Cp···dmit	5.2
(1 − x, 0.5 + y, 1.5 − z) and (1 − x, −0.5 + y, 1.5 − z)	Cp···Cp	11.4

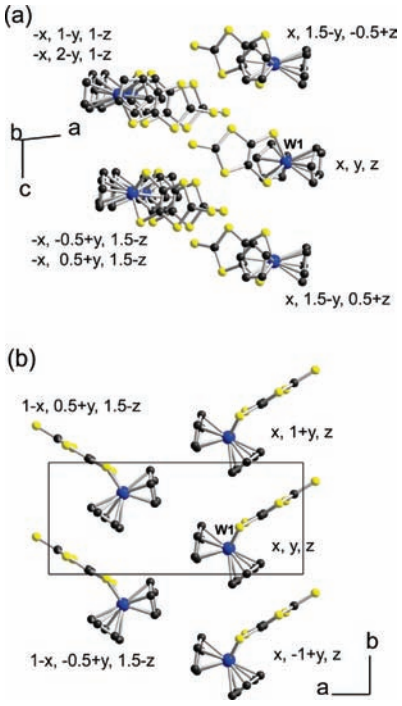

Figure 11. Details of the intermolecular interactions between one [Cp_2W(dmit)] complex at (x, y, z) and neighboring complexes in [Cp_2W(dmit)]Br (see also Table 8).

the monoclinic system, space group $P2_1/c$, with both the cation and anion in a general position in the unit cell. As shown in Figure 9, the cations are associated into layers perpendicular to a, with the bromide anions hydrogen bonded to the organometallic cations through C−H···Br^- interactions with the hydrogen atoms of the cyclopentadienyl rings (Figure 10 and Table 6).

A complex set of intermolecular interactions characterizes the structure of the Br^- salt as a given cation radical exhibits short intermolecular contacts with 10 neighboring molecules (Figure 11). As for the BF_4^- salt, calculations of the $\beta_{HOMO-HOMO}$ interaction energies were performed in the frame of extended Hückel tight binding methods, and the results are collected in Table 7. One observes that the stronger interactions develop within the bc plane through S···S and Cp···dmit interactions (along b) while these planes are connected to each other through Cp···Cp interactions.[37] This gives rise to a three-dimensional interaction network, as the interlayer Cp···Cp interaction is not negligible.

The temperature dependence of the magnetic susceptibility of [Cp_2W(dmit)]Br is shown in Figure 12. It exhibits

(37) Such intermolecular Cp···Cp interactions have been also observed, to a much stronger extent, in other heteroleptic complexes such as [CpNi(dithiolene)]. See: Fourmigué, M.; Cauchy, T.; Nomura, M. *CrystEngComm*. **2009**, *11*, 1491 and references therein.

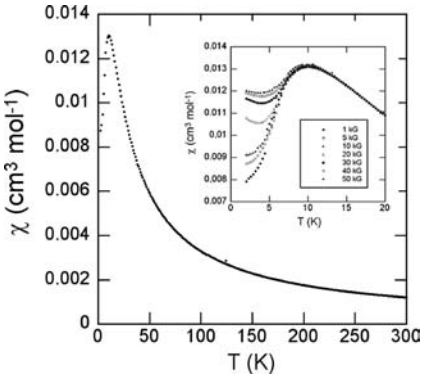

Figure 12. Temperature dependence of the susceptibility of [Cp_2W(dmit)]Br at 5 kG. Inset: Field dependence of the susceptibility below 20 K.

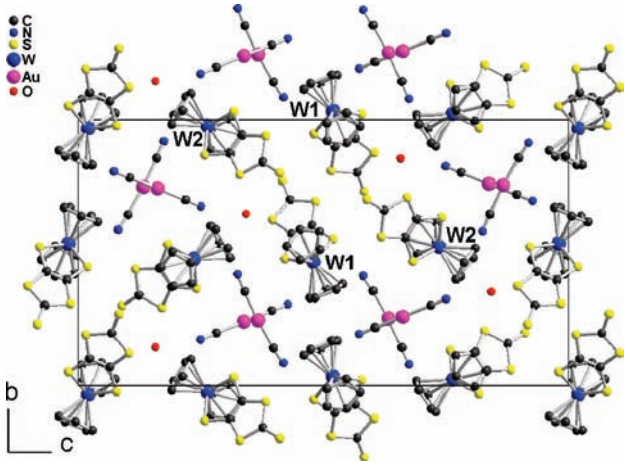

Figure 13. Projection view along a of the unit cell of [Cp_2W(dmit)][Au(CN)$_2$]·(H$_2$O)$_{0.5}$.

Table 8. Calculated $\beta_{HOMO-HOMO}$ Interaction Energies between the Two Crystallographically Independent Complexes (Noted **W1** and **W2**) and Their Neighbors within the Tetrameric Columns in [Cp_2W(dmit)][Au(CN)$_2$]

interacting complexes	interaction	β (meV)
W1(x, y, z) vs **W1**(1 + x, y, z)	Cp/dmit	28.6
W2(x, y, z) vs **W2**(1 + x, y, z)	Cp/dmit	51.1
W1(x, y, z) vs **W1**(−0.5 + x, 1.5 − y, 1 − z)	S···S	34.6
W1(x, y, z) vs **W2**(x, y, z)	S···S	12.1
W1(x, y, z) vs **W2**(1.5 + x, 1.5 − y, 1 − z)	S···S	16.3
W1(x, y, z) vs **W2**(0.5 + x, 1.5 − y, 1 − z)	S···S	4.8

a maximum at 10.6 K, confirming the presence of weak intermolecular antiferromagnetic interactions, while a fit to the Curie−Weiss law for T > 20 K gives a Curie−Weiss temperature θ_W = −14.5(1) K. At the lower temperatures, the magnetic susceptibility exhibits a field dependence (Figure 12 inset) indicative of the presence of an antiferromagnetic ground state below $T_{Néel}$(W) = 7 K.

Table 9. Crystallographic Data of the $[Cp_2W(dmit)][X]$ Salts

X^-	BF_4^-	PF_6^-	Br^-	$[Au(CN)_2]^-$
formula	$C_{13}H_{10}BF_4S_5W$	$C_{13}H_{10}F_6PS_5W$	$C_{13}H_{10}BrS_5W$	$C_{30}H_{20}Au_2N_4OS_{10}W_2$
formula mass	597.17	655.33	590.27	1534.82
cryst syst	monoclinic	monoclinic	monoclinic	orthorhombic
space group	$P2_1/c$	$P2_1/c$	$P2_1/c$	$P2_12_12_1$
a/Å	6.5630(2)	6.6514(7)	16.705(3)	7.5820(5)
b/Å	15.3090(3)	15.680(1)	7.279(1)	16.438(3)
c/Å	17.1500(4)	17.442(2)	12.856(3)	30.473(4)
α/deg	90.0	90.0	90.0	90.0
β/deg	92.200(3)	90.861(13)	96.26(3)	90.0
γ/deg	90.0	90.0	90.0	90.0
V/Å^3	1721.8(7)	1818.9(3)	1553.8(5)	3798.0(9)
Z	4	4	4	4
d_{calc}/g cm^{-3}	2.304	2.393	2.523	2.684
μ/mm^{-1}	7.348	7.067	10.662	14.322
data collected	23978	17078	21364	34983
ind. data	3948	4347	3562	8671
R_{int}	0.0297	0.1046	0.0325	0.0632
obs. data ($I > 2\sigma(I)$)	3259	3113	3135	6118
params refined	191	235	181	443
$R(F)$	0.0282	0.0462	0.0178	0.0416
$wR(F^2)$	0.0790	0.1109	0.0355	0.0690
residual d/e Å^{-3}	1.538, −0.917	2.944, −1.269	0.412, −0.787	1.642, −0.718

This behavior is fully coherent with the analysis of a three-dimensional set of intermolecular interactions reported above and also follows the behavior of the isostructural molybdenum salt[3b] $[Cp_2Mo(dmit)]Br$ where $\theta_{Mo} = -20$ K with a similar antiferromagnetic ground state below $T_{Néel}(Mo) = 4.5$ K.

$[Cp_2W(dmit)][Au(CN)_2]$. The solid state structure of the $[Au(CN)_2]^-$ salt is more complex than that of the three other BF_4^-, PF_6^-, and Br^- salts described above. Indeed, $[Cp_2W(dmit)][Au(CN)_2]\cdot(H_2O)_{0.5}$ (Figure 13) crystallizes in the orthorhombic system, space group $P2_12_12_1$, with two crystallographically independent $[Cp_2W(dmit)]^{+\bullet}$ cations as well as two crystallographically independent $[Au(CN)_2]^-$ anions and one water molecule, hydrogen bonded to the nitrogen atom of a cyanide moiety with a O···N distance of 2.84(2) Å and a O···N≡C angle of 157(1)°. The shortest Au···Au distance amounts to 3.28 Å, with a C−Au···Au′−C′ torsion angle of 85°, compatible with the presence of an aurophilic interaction. Such aurophilic interactions are often found with gold(I) species such as $[Au(CN)_2]^-$, with distances as short as 3.10 Å.[38,39] The longer distance found here is to be correlated also with the C−Au···Au′−C′ torsion angle. Indeed, theoretical studies and experimental results have shown that the Au···Au distances decrease with an increase in the torsion angle between adjacent $[Au(CN)_2]^-$ units.[40] The projection of the unit cell along a (Figure 13) shows that the radical cations are organized into columns running along a, associated four-by-four, and isolated from other 4-fold columns by the $[Au(CN)_2]^-$ and water molecules. Within these tetrameric columns, $\beta_{HOMO-HOMO}$ interactions energies were calculated and collected in Table 8. We found sizable interactions along the columns through Cp/dmit overlap combined with lateral interactions in between the columns through short S···S intermolecular contacts. This complex set of interactions cannot be summarized into a simple model such as a dimer, spin chain, or spin ladder. The temperature dependence of the magnetic susceptibility (Figure 14) is characterized with a susceptibility maximum at a low temperature (7.5 K), without any field dependence, an indication of the absence of an ordered three-dimensional ground state, in accordance with the essentially isolated tetrameric columns. On the basis of the calculated antiferromagnetic interactions within dyads (Table 8), a fit of the data was obtained from eq 3 involving antiferromagnetically coupled $S = 1/2$ dimers with a singlet ground state, with added contributions of a Curie tail at lower temperatures and of weaker interactions between dimers, giving $\rho = 0.062(5)$, $J/k_B = -7.26(7)$ K, and $J'/k_B = -2.19(1)$ K with $z = 6$.

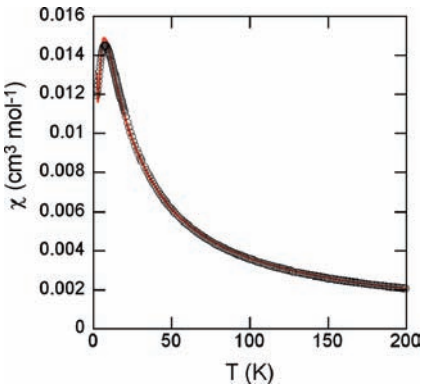

Figure 14. Temperature dependence of the magnetic susceptibility of $[Cp_2W(dmit)][Au(CN)_2]$ at 5000 G. The solid line is the best fit obtained by using eq 3, $R = 0.99947$.

(38) (a) Suarez-Varela, J.; Mota, A. J.; Aouryaghal, H.; Cano, J.; Rodriguez-Dieguez, A.; Luneau, D.; Colacio, E. *Inorg. Chem.* **2008**, *47*, 8143. (b) Suarez-Varela, J.; Sakiyama, H.; Cano, J.; Colacio, E. *Dalton Trans.* **2007**, 249.

(39) (a) Leznoff, D. B.; Lefebvre, J. *Gold Bull.* **2005**, *38*, 47 and references therein. (b) Zhou, H.-B.; Wang, S.-P.; Dong, W.; Liu, Z.-Q.; Wang, Q.-L.; Liao, D.-Z.; Jiang, Z.-H.; Yan, S.-P.; Cheng, P. *Inorg. Chem.* **2004**, *43*, 4552. (c) Colacio, E.; Lloret, F.; Kivekäs, R.; Suarez-Varela, J.; Sundberg, M. R.; Uggla, R. *Inorg. Chem.* **2003**, *42*, 560. (d) Lefebvre, J.; Callaghan, F.; Katz, M. J.; Sonier, J. E.; Leznoff, D. B. *Chem.—Eur. J.* **2006**, *12*, 6248. (e) Lefebvre, J.; Chartrand, D.; Leznoff, D. B. *Polyhedron* **2007**, *26*, 2189. (f) Katz, M. J.; Kaluarachchi, H.; Batchelor, R. J.; Bokov, A. A.; Ye, Z.-G.; Leznoff, D. B. *Angew. Chem., Int. Ed.* **2007**, *46*, 8804.

(40) (a) Colacio, E.; Lloret, F.; Kivekäs, R.; Suarez-Varela, J.; Sundberg, M. R. *Chem. Commum.* **2002**, 592. (b) Assefa, Z.; Omary, M. A.; McBurnett, B. G.; Mohamed, A. A.; Patterson, H. H.; Staples, R. J., Jr. *Inorg. Chem.* **2002**, *41*, 6274.

Conclusions

Several features have been identified here from the combination of spectroscopic, structural, and magnetic investigations performed on four novel $[Cp_2W(dmit)]^{+\bullet}$ cation radical salts. Comparison with analogous Mo salts shows that a recurrent trend toward more folded metallacycle geometry is observed with most W complexes, a consequence of stronger interactions between the CpW and dithiolene fragment orbitals. This is also associated with a smaller electronic contribution of the dithiolene fragment in the SOMO, as evidenced from the calculated charge distribution, and the smaller frequency shift upon folding exhibited by Raman-active C−S bands ($-10\ cm^{-1}$ vs $-15\ cm^{-1}$ in the W vs the Mo complex when going from $\theta = 0°$ to $\theta = 30°$). In that respect, the unfolded structure of the AsF_6^- salt appears as an anomaly, and it is anticipated that this structure actually distorts upon cooling, as already observed in the unfolded PF_6^- and AsF_6^- salts of the Mo analog, $Cp_2Mo(dmit)$.[3a] The magnetic behavior of the different salts also demonstrates that the spin density on the dithiolene moiety is strongly decreased in the W complexes, when compared with analogous Mo complexes, as the antiferromagnetic interactions which characterize these systems, are systematically weaker with the former, whatever the dimensionality of these interactions, 1D or 3D.

Experimental Section

The neutral $[Cp_2W(dmit)]$ and $[Cp_2Mo(dmit)]$ were prepared according to published procedures.[2,4] As electrolytes used in the electrocrystallization experiments, $[n\text{-}Bu_4N][BF_4]$, $[n\text{-}Bu_4N][PF_6]$, and $[PPh_4][Br]$ were commercially available; $[n\text{-}Bu_4N][Au(CN)_2]$ was prepared from the commercially available potassium salt $KAu(CN)_2$. Elemental analyses were performed at the Service de Microanalyse, ICSN, Gif/Yvette, France.

Electrocrystallization Experiments. General. All electrocrystallization experiments were performed in a galvanostatic mode with two-compartment cells and platinum wire electrodes (2-cm-long, 1 mm in diameter) under thermostatted conditions. Details on the solvent, concentration, temperature, and current used are given below for each system.

$[Cp_2W(dmit)][BF_4]$. The 1:1 salt was grown using the electrocrystallization method involving constant current oxidation of $Cp_2W(dmit)$ (15 mg) in the presence of electrolytic solutions prepared by dissolving $[n\text{-}Bu_4N][BF_4]$ (0.16 g, 0.5 mmol) in 10 mL of freshly distilled CH_2Cl_2 to yield an electrolyte solution with a final concentration of 0.5 M. Single crystals were grown at a constant current density of 5 μA at a temperature of 5 °C. Black block-like crystals were harvested from the anodic compartment of the electrochemical cell after a period of one week and washed with small amounts of freshly distilled CH_2Cl_2. Elem Anal. Calcd for $C_{13}H_{10}BF_4S_5W$ (MW = 597.2070 g/mol): C, 26.15%; H, 1.69%. Found: C, 25.93; H, 1.68. IR (KBr, cm^{-1}) 3088, 3132, 3144 (s, C−H stretch.), 1337 (s, C═C stretch.), 1028 (m, C═S stretching), 923 (w, C−S stretch.)

$[Cp_2W(dmit)][PF_6]$. $Cp_2W(dmit)$ (10 mg) was oxidized by galvanostatic current in an electrolyte solution prepared by dissolving $[Bu_4N][PF_6]$ (0.2 g) in 10 mL of freshly distilled CH_2Cl_2 at a constant current of 3 μA at room temperature. After one week, black needle-like crystals of the 1:1 salt were harvested from the anodic compartment of the electrochemical cell and washed with small amounts of freshly distilled CH_2Cl_2. Elem Anal. Calcd for $C_{13}H_{10}F_6PS_5W$ (MW = 655.3666 g/mol): C, 23.83%; H, 1.54%. Found: C, 23.83; H, 1.44. IR (KBr, cm^{-1}) 3093, 3122, 3138 (s, C−H stretch.), 1338 (s, C═C stretch.), 1030 (m, C═S stretch.), 923 (w, C−S stretching), 825, 842, 860 (s, PF_6^- f1u.)

$[Cp_2W(dmit)][Br]$. $Cp_2W(dmit)$ (22.1 mg) was oxidized by galvanostatic current in an electrolyte solution (0.5 M) prepared by dissolving $[PPh_4][Br]$ (0.2103 g, 0.501 mmol) in 10 mL of freshly distilled CH_2Cl_2 at a constant current of 5 μA at a temperature of −10 °C. After one week, black needle-like crystals of the 1:1 salt were harvested from the anodic compartment of the electrochemical cell and washed with small amounts of freshly distilled CH_2Cl_2. Elem Anal. Calcd for $C_{13}H_{10}BrS_5W$ (MW = 590.3064 g/mol): C, 26.45%; H, 1.71%. Found: C, 26.29; H, 1.60. IR (KBr, cm^{-1}) 3053, 3100 (s, C−H stretch.), 1348 (s, C═C stretch.), 1025 (m, C═S stretching), 911 (w, C−S stretch.).

$[Cp_2W(dmit)][Au(CN)_2]$. $Cp_2W(dmit)$ (14.6 mg) was oxidized in an electrolyte solution (0.5 M) prepared by dissolving $[n\text{-}Bu_4N][Au(CN)_2]$ (0.2464 g, 0.502 mmol) in 10 mL of freshly distilled CH_2Cl_2. Black needle-like single crystals of the 1:1 salt were grown using Pt electrodes at a constant current of 2 μA at 2 °C, harvested after a period of one week, and washed with small amounts of freshly distilled CH_2Cl_2. Elem Anal. Calcd for $C_{15}H_{10}AuN_2S_5W$ (MW = 759.4043 g/mol): C, 23.72%; H, 1.33%. Found: C, 23.60; H, 1.35. IR (KBr, cm−^{1}) 3055, 3069, 3088, 3121, 3134 (s, C−H stretching), 2138 (s, C≡N stretching), 1333, 1341, 1346 (s, C═C stretching), 1027 (w, C═S stretching), 923 (w, C−S stretching).

DFT Calculations. The quantum chemical calculations of both the neutral complex and the $[Cp_2W(dmit)]^{+\bullet}$ cation were carried out by using the Gaussian 3.0 program.[41] The equilibrium geometry and vibrational transitions were evaluated by the B3LYP and B3PW91 functionals with the LanL2DZ basis set, in the gas phase. Molecular and vibrational properties of the $[Cp_2W(dmit)]^{+\bullet}$ cation with different folding angles (θ) were also studied. In this case, the folding angle was fixed ($\theta = 0$, 10, 20, 30°), and then the geometry optimization process was performed.

Raman Spectroscopy. Raman spectra of single crystals were recorded at room temperature in a backward scattering geometry using a Labram HR HORIBA Jobin Yvon spectrometer with a He−Ne laser ($\lambda_{exc} = 632.8$ nm). The spectra were measured for different orientations of the electrical vector of the exiting laser beam: either parallel or perpendicular to the direction corresponding to maximum intensity of the Raman bands assigned to C═C stretching vibration. The spectra were mainly recorded within the range of strongest vibrational features, i.e., over the wavenumber range 150−2000 cm^{-1}. The power of the laser beam was about 0.1 mW, and the spectral resolution was 2 cm^{-1}.

Crystallography. Experimental data and refinement results are given in Table 9. Data were collected on an APEX II Bruker AXS diffractometer with Mo Kα radiation ($\lambda = 0.71073$ Å). Structures were solved by direct methods (SHELXS97[42] or SIR92)[43] and refined (SHELXL-97)[42] by full-matrix least-squares methods as implemented in the WinGX software package.[44] An empirical absorption (multiscan) correction was applied.

(41) Frisch, M. J.; Trucks, G. W.; Schlegel, H. B.; Scuseria, G. E.; Robb, M. A.; Cheeseman, J. R.; Montgomery, J. A., Jr.; Vreven, T.; Kudin, K. N.; Burant, J. C.; Millam, J. M.; Iyengar, S. S.; Tomasi, J.; Barone, V.; Mennucci, B.; Cossi, M.; Scalmani, G.; Rega, N.; Petersson, G. A.; Nakatsuji, H.; Hada, M.; Ehara, M.; Toyota, K.; Fukuda, R.; Hasegawa, J.; Ishida, M.; Nakajima, T.; Honda, Y.; Kitao, O.; Nakai, H.; Klene, M.; Li, X.; Knox, J. E.; Hratchian, H. P.; Cross, J. B.; Adamo, C.; Jaramillo, J.; Gomperts, R.; Stratmann, R. E.; Yazyev, O.; Austin, A. J.; Cammi, R.; Pomelli, C.; Ochterski, J. W.; Ayala, P. Y.; Morokuma, K.; Voth, G. A.; Salvador, P.; Dannenberg, J. J.; Zakrzewski, V. G.; Dapprich, S.; Daniels, A. D.; Strain, M. C.; Farkas, O.; Malick, D. K.; Rabuck, A. D.; Raghavachari, K.; Foresman, J. B.; Ortiz, J. V.; Cui, Q.; Baboul, A. G.; Clifford, S.; Cioslowski, J.; Stefanov, B. B.; Liu, G.; Liashenko, A.; Piskorz, P.; Komaromi, I.; Martin, R. L.; Fox, D. J.; Keith, T.; Al-Laham, M. A.; Peng, C. Y.; Nanayakkara, A.; Challacombe, M.; Gill, P. M.W.; Johnson, B.; Chen, W.; Wong, M. W.; Gonzalez, C.; Pople, J. A. *Gaussian 03*, revision B.05; Gaussian Inc.: Pittsburgh, PA, 2003.

(42) Sheldrick, G. M. *SHELX97*, release 97−2; University of Göttingen: Göttingen, Germany, 1998

Hydrogen atoms were introduced at calculated positions (riding model) included in structure factor calculation but not refined.

Acknowledgment. We thank T. Guizouarn (Rennes) for the SQUID measurements, D. Łazarski (Poznań) for help in Raman measurements, and B. Domercq (Nantes) for the first preparation of the $[Cp_2W(dmit)][PF_6]$ salt. This work was supported by the French−Polish program Polonium (no. 20083YF), and the French Ministry of Foreign Affairs (Postdoctoral fellowship to E.W.R.). We also thank the Polish Ministry of Science and Higher Education for the research project in the years 2008−2010.

Supporting Information Available: A crystallographic file in CIF format is provided. This material is available free of charge via the Internet at http://pubs.acs.org.

(43) Altomare, A.; Burla, M. C.; Camalli, M.; Cascarano, G. L.; Giacovazzo, C.; Guagliardi, A.; Moliterni, A. G. G.; Polidori, G.; Spagna, R. *J. Appl. Crystallogr.* **1999**, *32*, 115–119.
(44) Farrugia, L. J. *J. Appl. Crystallogr.* **1999**, *32*, 837–838.